Lone-Pair Orbital Interactions in Polythiaadamantanes

Joseph E. Norton, Alejandro L. Briseno, Fred Wudl, and K. N. Houk*

Department of Chemistry and Biochemistry, University of California, Los Angeles, California 90095-1569

Received: March 6, 2006; In Final Form: June 12, 2006

The electronic structures of a series of polythiaadamantanes from thiaadamantane through 2,4,6,8,9,10-hexathiaadamantane (HTA) have been analyzed using density functional theory calculations in conjunction with Hückel and natural bond orbital analysis. The effects of multiple sulfur p-type lone-pair orbital interactions on ionization potentials, hole mobilities, and electronic coupling have been determined. An overall increase in the average energy of the lone-pair orbitals as the number of sulfur atoms increases is predicted, with the exact positioning of the HOMO depending on specific lone-pair interactions. Separation of through-bond (TB) and through-space (TS) interactions between intramolecular sulfur atoms has been performed using localized molecular orbitals and model systems based on interacting hydrogen sulfide molecules. TB interations were found to reduce orbital splitting, while TS interactions were found to increase orbital splitting. TS interactions were more or less constant from one polythiaadamantane to the next, and the contributions of TB effects to individual orbital energies vary depending on the relative orientation of sulfur atoms as determined by the σ molecular framework. Electronic coupling between intermolecular sulfur lone-pair orbitals was determined by investigating unique dimer pairs observed in the crystal structure of HTA. Electronic coupling is not as strong as expected given the short intermolecular S−S distances observed in the crystal structure. In general, B3LYP/6-31G(d) and B3LYP/6-311+G(d,p) give very similar orbital energies and splittings.

Introduction

Intramolecular interactions between molecular orbitals in polyatomic molecules are important in understanding the nature of electronic structures. These interactions are traditionally classified as being either through-bond (TB) or through-space (TS), where TS interactions occur directly between nearby orbitals and TB interactions result from coupling effects that occur indirectly through the σ-bond skeleton.[1−3] Competition between TB and TS interactions has been shown to be important in determining the electronic properties of systems such as aryne biradicals,[3−5] diene hydrocarbons,[6] cyclic polyenes,[7] and norbornadiene[1,2,8−13] and its derivatives.[14] It is often found that interesting orbital interactions occur in systems with unusual topologies where strong orbital interactions exist.

We have analyzed the electronic structures of a series of polythiaadamantanes from thiaadamantane through 2,4,6,8,9,-10-hexathiaadamantane (HTA). The effects of orbital interactions on ionization potentials, hole mobilities, and electronic coupling have been determined. HTA is a highly symmetric molecule consisting of a tricyclic array of interacting sulfur lone-pair orbitals with short intermolecular sulfur distances. The sulfur atoms contain p-type lone pairs that extend into the interior of the molecule and interact with the σ framework. To determine the effects of these interactions, the electronic properties of HTA and polythiaadamantanes were investigated by separating TB and TS interactions between intramolecular sulfur atoms using natural bond orbital (NBO) analysis[15−18] and model systems based on interacting hydrogen sulfide molecules. Hückel molecular orbital (HMO) analysis of the model systems is performed on orbital splitting patterns determined from density functional theory (DFT) calculations. Hole mobility is approximated by calculating electronic coupling between unique dimer pairs from a newly reported crystal structure of HTA. The use of Kohn−Sham (KS) orbital energies of DFT has been a source of concern, since it is often thought that KS orbitals are merely auxiliary components that carry no definite physical meaning. However, contrary to this view, it has been argued that KS orbitals do carry physical meaning and are suitable for use in qualitative molecular orbital theory.[19−25] Taking this into account, we use DFT orbital energies here and have relegated Hartree−Fock (HF) orbital energies to the Supporting Information.

The crystal structure of HTA was first determined in 1956.[26,27] The crystal forms a tetragonal lattice with intermolecular S−S distances as short as 3.52 and 3.59 Å,[26,27] whereas, in adamantane, the shortest C−C distance is 3.93 Å and the shortest distance between two hydrogens is 2.37 Å.[28] Considering that the molecular symmetry of HTA is T_d, one might expect an even higher symmetry for the crystals, given that both adamantane and hexamethylene tetramine have T_d symmetry and form cubic crystals.[29,30] However, replacement of methylene groups with sulfur atoms permits very close packing that leads to a less symmetric orientation of the molecules. Interactions between sulfurs of adjacent HTA molecules are strong, as indicated by the insolubility of its crystal, a decomposition temperature of 330 °C,[26] and intermolecular sulfur distances shorter than the van der Waals (vdW) distance expected for two sulfur atoms (3.6 Å). HTA and analogous ring systems such as adamantane, hexamethylene tetramine,[31] and derivatives of polythiaadamantanes have been studied and are shown in Chart 1. Of these, HTA is the most stable.

The molecule 2,4,6,8,9,10-hexathiaadamantane forms a stable and well-organized crystal that might be expected to have interesting electronic properties attractive for applications in semiconducting organic materials. The presence of strong

* Corresponding author. Telephone: 310-206-0515. Fax: 310-206-1843. E-mail: houk@chem.ucla.edu.

10.1021/jp061385w CCC: $33.50
Published on Web 07/25/2006

CHART 1

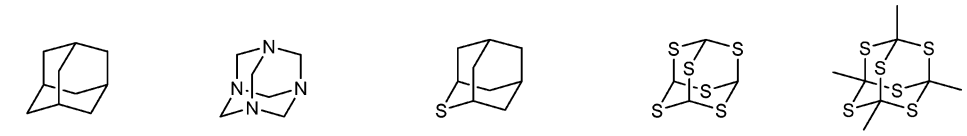

Adamantane | Hexamethylene tetramine | Mono-thiaadamantane | Hexa-thiaadamantane (HTA) | Tetramethyl HTA

TABLE 1: HF/6-31G(d) and B3LYP/6-31G(d) Calculated Ionization Potentials (IP_{KT} and $IP_{\Delta E}$) Obtained from Koopmans' Theorem and the ΔE Method for Dialkyl Sulfides (R−S−R′)

		HF/6-31G(d)		B3LYP/6-31G(d)			
R	R′	IP_{KT} (eV)	$IP_{\Delta E}$ (eV)	IP_{KT} (eV)	$IP_{\Delta E}$ (eV)	IP_{exp} (eV)	$\langle IP_{exp} \rangle$ (eV)
H	H	10.44	9.26	7.12	10.38	10.48[a]	10.48
Me	H	9.69	8.38	6.43	9.38	9.42[b]	9.42
Me	Me	9.09	7.68	5.91	8.62	8.68,[a] 8.65,[b] 8.77,[c] 8.67 [d]	8.69
Me	Et	9.03	7.54	5.85	8.47	8.55[e]	8.55
Et	Et	8.97	7.41	5.80	8.33	8.48,[a] 8.56,[c] 8.44[e]	8.49
Et	Pr	8.95	7.35	5.78	8.27	8.50,[c] 8.37[e]	8.44
Pr	Pr	8.93	7.30	5.77	8.21	8.45[c]	8.45
Bu	Bu	8.91	7.24	5.75	8.15	8.40[c]	8.40
Pr	i-Bu	8.90	7.24	5.75	8.14	8.40[c]	8.40
i-Bu	i-Bu	8.85	7.14	5.69	8.03	8.36,[c] 8.20[e]	8.28
i-Pr	i-Pr	8.94	7.24	5.79	8.13	8.26,[a] 8.38[c]	8.32
t-Bu	*t*-Bu	8.87	7.03	5.72	7.92	8.07 [a]	8.07

[a] References 39−41. [b] Reference 42. [c] Reference 43. [d] Reference 44. [e] Reference 45.

interactions between lone-pair orbitals of polarizable sulfur atoms suggests that if HTA is easily oxidizable, its crystal structure could perform ideally as a three-dimensional conducting crystal with hole mobilities adequate for electroactive materials applications. However, the electronic structures and properties of HTA and other polythiaadmantanes have been relatively unexplored despite having a highly symmetric rigid molecular framework where orbital interactions can be systematically investigated.

Computational Methods

Calculations were performed using Gaussian 03[32] and the hybrid density functional Becke3LYP[33,34] with the 6-31G(d) and 6-311+G(d,p) basis sets. Geometry optimizations were carried out on each polythiaadamantane and were followed by frequency calculations in order to verify that stationary points obtained were true energy minima. Ionization potentials (IP) were determined using Koopmans' theorem[35] and the ΔE method with the HF/6-31G(d) and B3LYP/6-31G(d) methods. Polythiaadamantanes and corresponding model systems based on hydrogen sulfide molecules were used in conjunction with natural bond orbital[15−18] analysis to remove TB interactions and extract TS interactions. The NBO 3.0 software package incorporated into Gaussian 03 was used to analyze each polythiaadamantane. The model systems were optimized while holding the coordinates of each sulfur atom fixed and constraining all intermolecular bond angles and dihedrals. This effectively allowed the S−H bonds to relax. HTA dimer pairs were obtained from crystal structure data and optimized with fixed intermolecular bond distances, angles, and dihedrals involving the three closest intermolecular sulfur pairs. This allowed the individual monomers of the dimer pairs to relax while maintaining the intermolecular coupling interactions.

Results and Discussion

Ionization Potentials of Dialkyl Sulfides. Accurate determination of ionization energies is useful in exploring the electronic structures of molecules and ions in the gas phase. Theoretical approaches to predicting ionization energies are often used to interpret spectra and properly assign spectroscopic bands. Preliminary electrochemistry data and the investigation of p-type semiconducting devices using HTA as the functional material suggest that HTA is difficult to oxidize.[36] Therefore, our initial investigation consists of accurately determining the IPs of polythiaadamantanes. Ionization energies taken directly from the HOMO energy are known to be severely underestimated by exchange correlation functionals, such as B3LYP. However, the application of DFT to probe orbital interactions and IPs has been documented.[37] Hartree−Fock (HF) more accurately reproduces ionization energies based on the HOMO energy, but errors due to factors such as electronic relaxation effects become more severe depending on the nature and size of the studied molecules. To predict ionization energies for polythiaadamantanes, the ΔE method has been used where calculated IPs are obtained from the energy difference $E_{cation} - E_{neutral}$. This method is shown to give rather accurate values for first ionization energies of small molecules.[38] In this study, a series of dialkyl sulfides were used to calibrate this method for calculating IPs of polythiaadamantanes.

The experimental ionization energies of hydrogen sulfide, methanethiol, and 10 dialkyl sulfides ranging from dimethyl sulfide through di-*tert*-butyl sulfide are listed in Table 1. The ionization energies were also calculated using two methods. IP values were obtained directly from HOMO orbital energies based on Koopmans' theorem (IP_{KT}) or by the ΔE method ($IP_{\Delta E}$) using HF/6-31G(d) and B3LYP/6-31G(d) levels of theory. These methods were correlated with experimental values of dialkyl sulfides using an average IP in cases where multiple experimental values were available.[39−45] The plots of experimental IPs calculated from B3LYP/6-31G(d) and HF/6-31G(d) HOMO energies are shown in Figure 1. The B3LYP Kohn−Sham orbitals severely underestimate IP values, while HF underestimates these values less. The lower IP values ($IP_{exp} < 8.40$ eV) correspond to larger and more branched dialkyl sulfides containing *i*-Pr, *i*-Bu, and *t*-Bu substituents, for which both methods become increasingly far from experimental values.

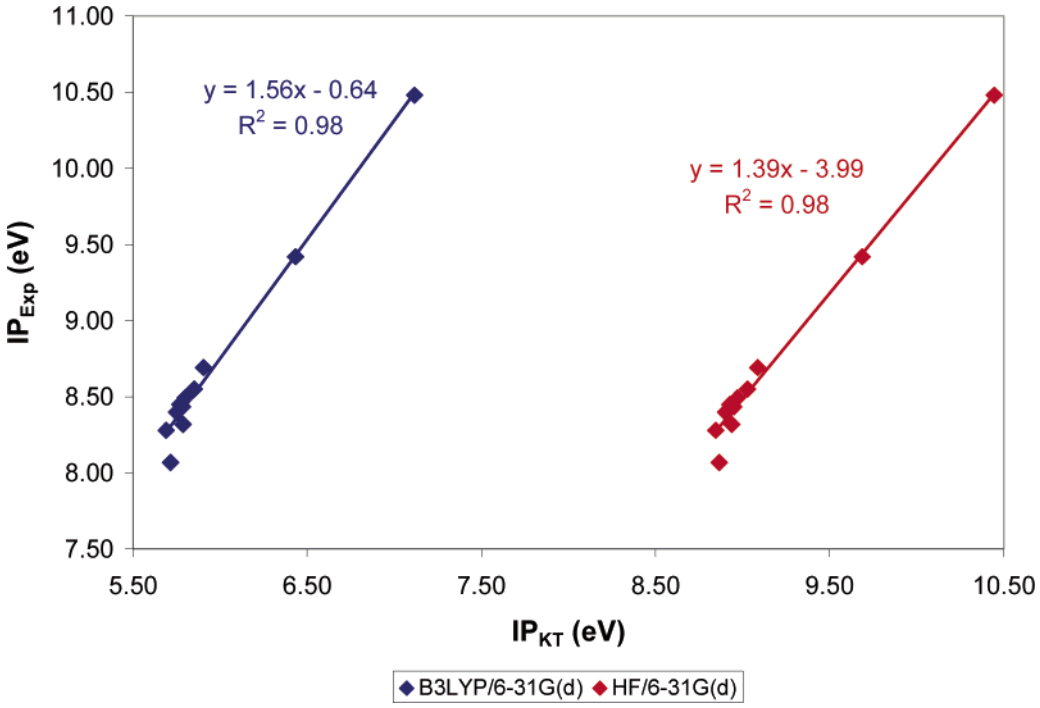

Figure 1. Plot of B3LYP/6-31G(d) and HF/6-31G(d) negative HOMO energies vs experimental IPs for dialkyl sulfides. Equations and R^2 values obtained from linear regression analysis are displayed on the graph.

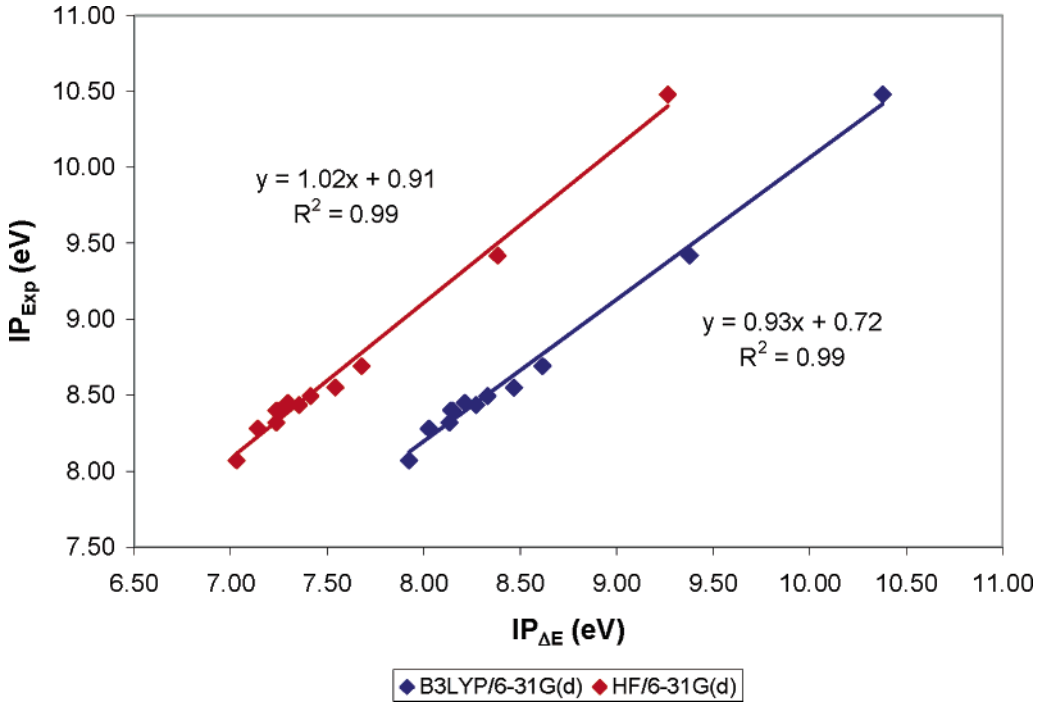

Figure 2. Plot of B3LYP/6-31G(d) and HF/6-31G(d) IPs obtained from the ΔE method vs experimental IPs for dialkyl sulfides. Equations and R^2 values obtained from linear regression analysis are displayed on the graph.

While R^2 values indicate fairly good correlation with experimental values, Koopmans' theorem becomes a poor predictor as the systems become large. In addition, trends obtained from linear regression analysis of B3LYP and HF data give slopes that deviate significantly from unity.

The plots of experimental IPs versus those calculated from the ΔE method are shown in Figure 2. Both levels of theory give very good correlations with experimental values, especially for larger systems, and slopes are close to unity. With the ΔE method, HF slightly underestimates ionization energies while B3LYP provides predictions closer to experimental values. From the methods examined here, the ΔE method using B3LYP/6-31G(d) ($R^2 = 0.99$) is the preferred method for predicting IPs for polythiaadamantanes.

Ionization energies for polythiaadamantanes were first calculated using the ΔE method and then corrected by the best-fit-line equation, $IP_{exp} = 0.93IP_{\Delta E} + 0.72$, obtained from the graph in Figure 2. The predicted values, $IP_{\Delta E,corr}$, for adamantane and mono- through hexathiaadamantane are shown in Figure 3. The IP of adamantane is known experimentally to be 9.2 eV and is predicted here to be slightly higher at $IP_{\Delta E,corr} = 9.41$ eV. The $IP_{\Delta E,corr}$ values for polythiaadamantanes range from

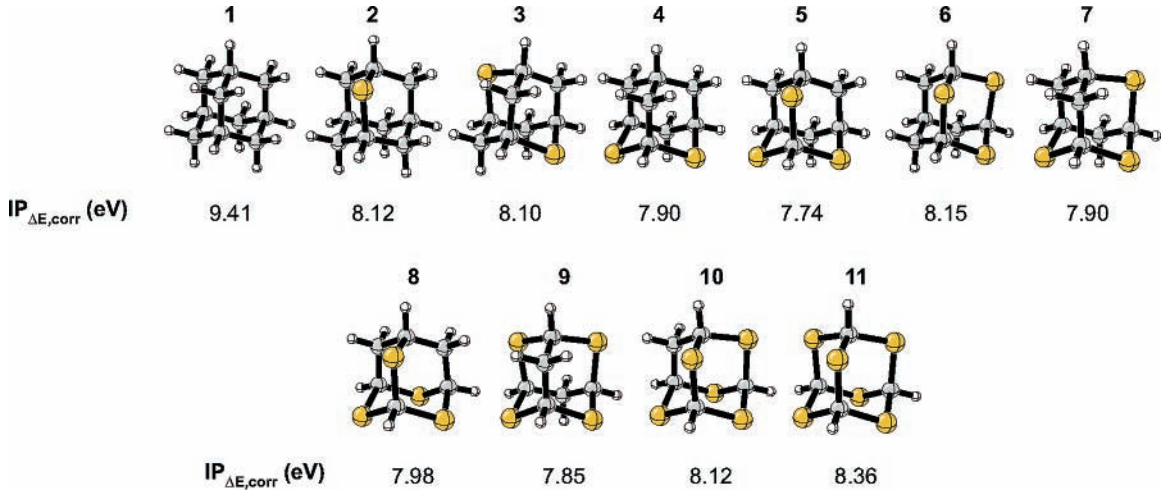

Figure 3. B3LYP/6-31G(d) ionization potentials ($IP_{\Delta E,corr}$) obtained from the ΔE method and the best-fit-line equation for adamantane (**1**), 2-thiaadamantane (**2**), 2,6-dithiaadamantane (**3**), 2,4-dithiaadamantane (**4**), 2,4,10-trithiaadamantane (**5**), 2,4,9-trithiaadamantane (**6**), 2,4,6-trithiaadamantane (**7**), 2,4,6,10-tetrathiaadamantane (**8**), 2,4,6,8-tetrathiaadamantane (**9**), 2,4,6,8,9-pentathiaadamantane (**10**), and 2,4,6,8,9,10-hexathiaadamantane (**11**). Energies are reported in electronvolts.

TABLE 2: B3LYP Through-Space (TS), Through-Bond (TB), and Net Orbital Splittings in Polythiaadamantanes

		orbital splitting energies (eV)					
		6-31G(d)			6-311+G(d,p)		
compound		TS[a]	TB[b]	Net	TS[a]	TB[b]	Net
2,6-dithiaadamantane	**3**	0.00	0.00	0.00	0.00	0.00	0.00
2,4-dithiaadamantane	**4**	1.21	−0.61	0.60	1.24	−0.63	0.61
2,4,10-trithiaadamantane	**5**	1.36	−0.51	0.85	1.36	−0.50	0.86
2,4,9-trithiaadamantane	**6**	1.63	−0.96	0.67	1.69	−0.99	0.70
2,4,6-trithiaadamantane	**7**	0.88	−0.45	0.43	0.89	−0.45	0.44
		0.82	−0.38	0.44	0.87	−0.42	0.44
2,4,6,10-tetrathiaadamantan e	**8**	0.46	−0.15	0.31	0.48	−0.16	0.31
		0.90	−0.36	0.53	0.87	−0.32	0.54
		0.51	−0.35	0.15	0.54	−0.37	0.16
2,4,6,8-tetrathiaadamantane	**9**	1.21	−0.60	0.61	1.25	−0.62	0.63
		1.27	−0.57	0.70	1.20	−0.51	0.69
2,4,6,8,9-pentathiaadamanta ne	**10**	0.15	−0.09	0.06	0.19	−0.12	0.06
		0.80	−0.28	0.52	0.77	−0.24	0.53
		0.72	−0.36	0.37	0.73	−0.35	0.37
		0.14	0.01	0.15	0.14	0.00	0.14
2,4,6,8,9,10-hexathiaadama ntane	**11**	1.58	−0.66	0.92	1.57	−0.64	0.93

[a] TS splitting energies were obtained from B3LYP/6-31G(d) calculations on the model H_2S dimers, trimer, tetramer, pentamer, and hexamer. [b] TB splitting energies were obtained from differences between the calculated TS splitting energies and the net splitting observed in polythiaadamantanes.

7.74 to 8.36 eV with trithiaadamantane **5** having the lowest IP and HTA (**11**), surprisingly, having the highest IP. This, along with the observed fluctuations in IPs in the series of polythiaadamantanes, is an indication of the interplay between specific orbital interactions and inductive effects of the sulfur atoms. A more detailed analysis is provided in the next section of this paper.

Separation of Through-Bond and Through-Space Interactions. Through-bond and through-space interactions are both expected to be significant in polythiaadamantanes, since lone-pair orbitals extend into the interior of the molecule and are most often separated by only two σ-bonds. The following analysis of OITS, OITB, and inductive effects attempts to separate the effect of these interactions on orbital energies of multiple interacting sulfur lone-pair electrons. Net orbital splitting energies associated with successively replacing each CH_2 of adamantane with sulfur were investigated by using DFT methods to explore polythiaadamantanes with various numbers of sulfur atoms. Geometries and orbital energies were compared in order to understand the exact positioning and extent of interaction between specific lone-pair orbitals.

The amount of orbital splitting due to TS interactions was determined by removing the carbon skeleton from each polythiaadamantane and replacing each sulfur with a H_2S molecule. The coordinates of each sulfur were fixed, and the intermolecular bond angles and dihedrals were constrained. The S−H bond distances were allowed to optimize. Since the orbital splitting in the H_2S model system is caused by TS interactions alone, splitting due to TB interactions can be extracted from the net orbital splittings of the polythiaadamantanes. This process was performed for each polythiaadamantane to calculate the TS and TB interaction energies that are listed in Table 2. The results from this analysis show that TS interactions generally contribute more to splitting than TB interactions, and TB interactions have an overall contribution in the opposite direction of TS interactions. TB interactions generally destabilize lower energy lone-pair orbitals or stabilize higher energy lone-pair orbitals and reduce splitting.

Visual inspection of B3LYP orbitals of polythiaadamantanes shows that two types of TB interactions are dominant. These are discussed in more detail as individual polythiaadamantanes are analyzed. For now, these interactions are depicted schematically in Figure 4. There are $n_S-\sigma$ repulsive interactions between

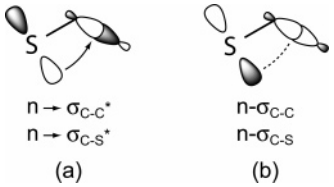

Figure 4. Orbital interactions consisting of (a) delocalization of lone-pair orbitals into σ^* orbitals and (b) repulsive interactions between lone-pair orbitals and neighboring σ bonds.

sulfur lone pairs and neighboring σ_{C-C} or σ_{C-S} bonds, and there are $n_S \rightarrow \sigma^*$ hyperconjugation interactions between lone pairs and adjacent σ_{C-C}^* or σ_{C-S}^* orbitals. TB $n_S - \sigma$ interactions are destabilizing because the lone-pair orbitals are destabilized by interaction with lower-lying σ orbitals. The $n_S \rightarrow \sigma^*$ interactions stabilize the n_S orbitals and involve delocalization of lone-pair electrons into vacant σ_{C-S}^* or σ_{C-C}^* orbitals. Investigation of each polythiaadamantane and results from NBO analysis are used below to provide a more detailed description of how these interactions influence orbital splitting.

Orbital Splitting and Hückel Analysis. Polythiaadamantanes are systems of interacting p orbitals that are, however, not part of a π system. These systems can be analyzed with methods similar to those used to analyze traditional π systems, although the overlap is different. Polythiaadamantanes actually exhibit interesting splitting patterns that can be explained using either group theory or a simple Hückel model. A simple Hückel model has been applied here to analyze the B3LYP/6-31G(d) through-space splitting energies of the H_2S model systems.[46−49]

Lone-pair electrons in polythiaadamantanes are arranged in a cyclic array that results in interactions that are intermediate between σ and π. As a consequence, the phase of the interacting resonance integral, β, of the lone-pair orbitals must be considered. In determining β for each system, the average energy of the lone-pair orbitals is used to determine α. In the Hückel model, interactions between adjacent p orbitals have energy of β, and all others are zero. For the H_2S model systems, the resonance integral is the interaction energy resulting strictly from TS interaction between adjacent lone pairs in the absence of a carbon framework and, therefore, will be represented as β_{TS} to designate through-space interaction. The B3LYP/6-31G(d) splitting patterns of H_2S models systems of mono- through hexathiaadamantane are shown in Figure 5. The splitting patterns are overlaid with the splitting patterns used to extract values for β_{TS} based on a Hückel model. Values of β_{TS} fluctuate between 0.62 and 0.40 eV with the lowest interaction energy occurring for hexathiaadamantane. Polythiaadamantanes were optimized first in order to generate H_2S model systems from which to extract TS interactions, as the S−S distances and angles are not identical in each system, leading to different values of β_{TS}.

Now that TS interactions have been obtained from the H_2S model systems, the effects of TS and TB interactions on individual orbitals can be dissected. To perform this analysis, a reference energy for orbital energies that lack both TS and TB interaction energies must be established. The NBO[15−18] method developed by Reed and Weinhold has been demonstrated to provide quantitative dissections of electronic energies.[14,50−55] The NBO method is used here to obtain localized molecular orbitals (LMO) that are assumed to have neither TS nor TB interactions. However, the localized molecular orbitals provided by NBO population analysis of canonical orbitals are in fact not completely localized on one center, since these "localized" molecular orbitals contain both orthogonalization and delocalization tails, the latter of which is a contribution of electronic delocalization into unfilled antibonding orbitals.[17] These effects can lead to nondegenerate NBO energies in some polythiaadamantanes, in which case, an average of NBO energies is used.

The procedure by which localized molecular orbitals from NBO analysis were combined with Hückel calculations on the H_2S model systems to extract TB interactions in individual lone-pair orbitals is shown in Figure 6. The energies of localized orbitals obtained from NBO analysis are indicated on the left side of the diagrams. The splitting observed in the H_2S model

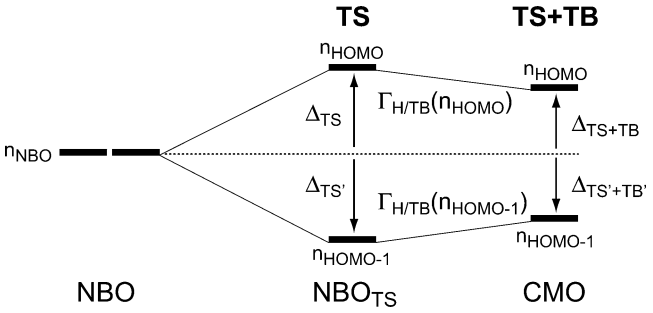

Figure 6. Schematic for extracting TS and TB interactions in polythiaadamantanes. Orbitals corresponding to n_{NBO} are localized molecular orbitals lacking TS and TB interactions. TS interaction energies obtained from splitting energies of H_2S model systems are applied to n_{NBO} energies to acquire energies for orbitals composed only of TS interactions, NBO_{TS}. Shifts in orbitals due to TB interactions are denoted $\Gamma_{H/TB}$ and are obtained from the differences between B3LYP canonical molecular orbitals (CMO) and NBO_{TS} energies.

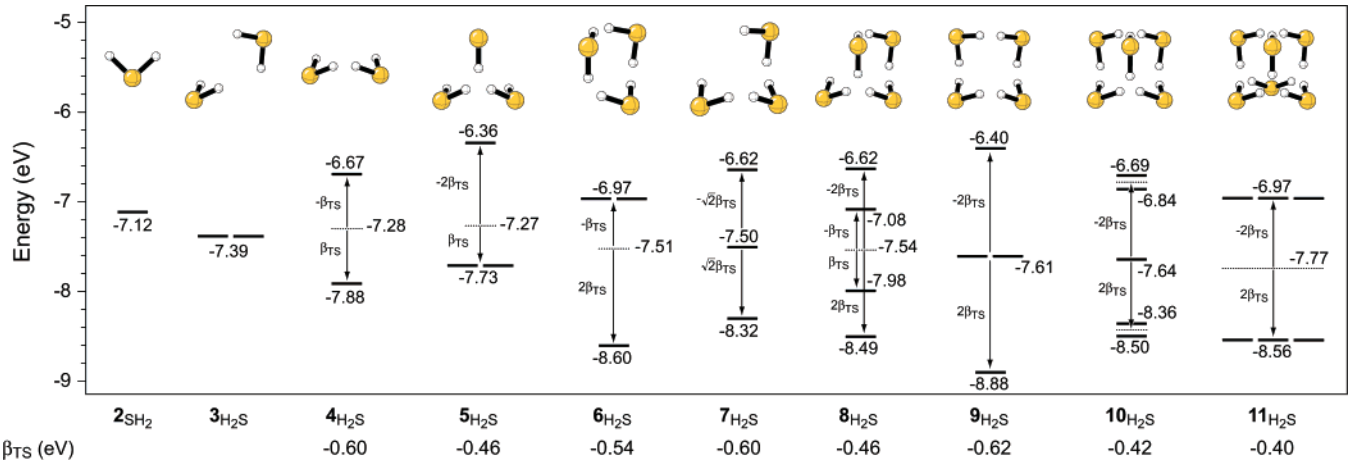

Figure 5. B3LYP/6-31G(d) orbital splitting patterns of H_2S model systems of polythiaadamantanes. Resonance energies extracted using Hückel analysis are denoted β_{TS}.

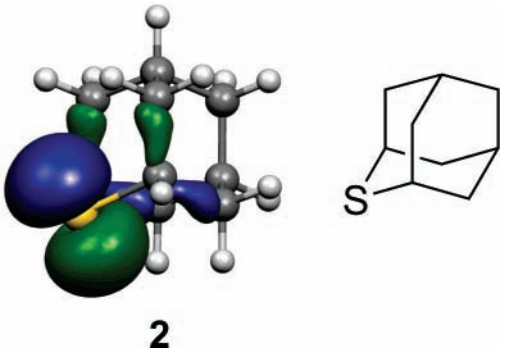

Figure 7. Lone-pair orbital of 2-thiaadamantane (**2**) demonstrates the $n_S-\sigma_{C-C}$ interactions between the lone-pair and proximal σ_{C-C} bonds.

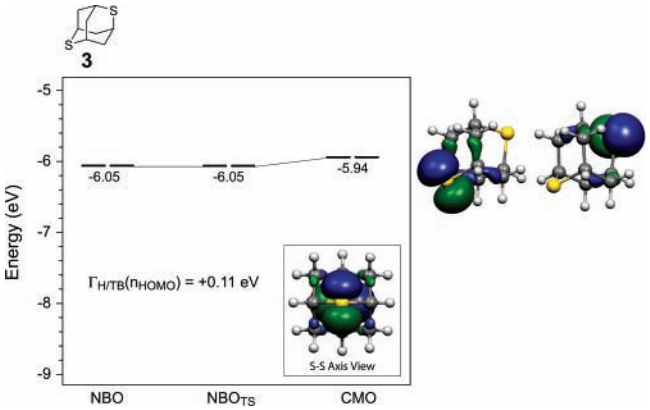

Figure 8. B3LYP/6-31G(d) orbital correlation diagram of 2,6-dithiaadamantane (**3**). The inset shows a view down the S−S axis of **3**. Molecular orbital energies are reported in electronvolts.

calculations are added to give the energies in the middle. This adjusts the orbital energies to the values they would have if the corresponding polythiaadamantane contained only TS interactions; these are denoted NBO_{TS} in Figure 6. The net splitting due to TS interactions is given as $\Delta_{TS} + \Delta_{TS'}$. The orbitals of the actual polythiaadamantane obtained from B3LYP/6-31G(d) are the canonical molecular orbitals (CMO), which contain both TS and TB interactions. The differences between the corresponding CMO and NBO_{TS} energies are the orbital shifts due to hyperconjugation and to TB interactions and are denoted by $\Gamma_{H/TB}$ designated with the appropriate orbital. The net splitting due to TS and TB interactions is given as Δ_{TS+TB}. The ordering of orbitals in polythiaadamantanes is consistent with that of the corresponding H_2S model systems; neither TS nor TB interactions are large enough to cause two orbitals to swap their energetic order.

The simplest polythiaadamantane, monosubstituted **2**, does not contain interacting sulfur atoms but does provide insight into the type of orbital interactions that will be encountered. The lone-pair orbital of **2** is shown in Figure 7 and clearly demonstrates the destabilizing (to n_S) $n_S-\sigma_{C-C}$ interactions present. These $n_S-\sigma_{C-C}$ interactions are responsible for destabilization of the lone pair orbital in addition to effects resulting from replacing the hydrogens of H_2S with a carbon skeleton. For comparison, the HOMO of H_2S is −7.12 eV and the HOMO of 2-thiaadamantane, **2**, is much higher at −5.68 eV, indicating that the carbon framework raises the HOMO through both inductive effects and direct interaction of the lone-pair orbital with σ-bonds. The discussion will use B3LYP/6-31G(d) energetics; it has been found that B3LYP/6-31G(d) and B3LYP/6-311+G(d,p) energies result in identical conclusions. The specific orbital, splitting, and average orbital energies of H_2S model systems and polythiaadamantanes with both methods are reported in Tables 3 and 4.

In the case of dithiaadamantanes, there is now potential for interaction between two sulfur atoms. In 2,6-dithiaadamantane, **3**, the sulfur atoms are distally located and are noninteracting due to symmetry, as can be seen by the degenerate HOMOs in Figure 8. The lone-pair orbitals are orthogonal, as shown in the inset of Figure 8. Even though splitting does not occur in **3**, there are $n_S-\sigma_{C-C}$ interactions that destabilize the HOMO by 0.11 eV when compared with the energy of the localized NBO shown in Figure 8. The HOMO of **3** is 0.26 eV lower than the HOMO of **2**, decreasing from −5.68 eV in 2-thiaadamantane to −5.94 eV in **3**. The orbital energies change by almost the same amount from −7.12 eV in the H_2S monomer to −7.39 eV, in the model H_2S dimer. The second sulfur produces an inductive effect that lowers the energy of the other sulfur lone pair.

In 2,4-dithiaadamantane **4**, the sulfurs are bound to a common carbon and interact to produce the splitting shown in Figure 9. Hückel analysis of the H_2S model system, $\mathbf{4}_{H_2S}$ in Figure 5, calculated β_{TS} to be −0.6 eV with a net splitting, $2\beta_{TS}$, of 1.2 eV. A decrease in the average energy of the lone-pair orbitals of the H_2S model system is observed upon addition of a second H_2S. This is the general trend for all of the model systems with the largest decrease occurring for the H_2S hexamer, which decreases by 0.65 eV from −7.12 eV in the monomer to −7.77 eV in the hexamer. For polythiaadamantanes, similar decreases are observed with the largest being for HTA (**11**), which decreases by 1.11 eV from −5.68 eV in 2-thiaadamantane to −6.79 eV in **11**.

The carbon skeleton of polythiaadamantanes introduces TB interactions that produce changes in the magnitudes of observed splittings. For example, the HOMO-1 of **4** involves substantial through-bond $n_S-\sigma_{C-C}$ interactions where the sulfur lone-pair orbitals mix with adjacent C−C σ-bond orbitals. For symmetry reasons, these interactions are absent in the HOMO, so that the decrease in orbital splitting arises primarily because of destabilization of the HOMO-1. The HOMO is antisymmetric with respect to the plane separating the two sulfur lone-pair orbitals and, therefore, does not involve mixing with the bonding orbitals of the central C−C σ-bond. There is a noticeable difference in the tilt of the lone-pair molecular orbitals. The bottom lobes of the HOMOs are tilted slightly inward toward the carbon joining the sulfurs as compared to the lone pair of the monothio compound (cf. Figures 7 and 9). The bottom lobes of the HOMO-1 are rotated outward quite dramatically and away from the central carbon. The perturbations of the HOMO-1 and the HOMO are reflected in the energetics of TB interactions: these are strong in the HOMO-1 and cause +0.59 eV of destabilization, as shown by $\Gamma_{H/TB}(n_{HOMO-1})$ in Figure 9, while the HOMO is relatively unaffected and stabilized by only −0.01 eV.

The slight tilting observed in the HOMO is due to delocalization of the lone pairs into the opposing σ^*_{C-S} bonds. NBO analysis predicts this type of interaction to occur more strongly than delocalization into σ_{C-C}* bonds. In the HOMO-1, the bonding combination of the lobes occurs and the lone pairs interact strongly with σ_{C-C} bonds of the molecule. The lone pairs mix mostly with the intervening σ_{C-C} bond between the two sulfurs.

The interaction of the lone-pair orbitals with the central σ_{C-C} bond is the primary contributor to TB effects in **4**. To model this interaction, $CH_3CH(SH)_2$, shown in the inset of Figure 9, was optimized with bond angles and dihedrals identical to those of **4**. A net n_S-n_S splitting of 0.73 eV occurs in this model.

TABLE 3: B3LYP Orbital Splitting Energies (eV) of Hydrogen Sulfide Model Systems

		6-31G(d)	6-311+G(d,p)			6-31G(d)	6-311+G(d,p)
$\mathbf{2}_{H_2S}$	$E(n_{HOMO})$	−7.12	−7.28	$\mathbf{9}_{H_2S}$	$E(n_{HOMO})$	−6.40	−6.43
3_{H_2S}	$E(n_{HOMO})$	−7.39	−7.53		$E(n_{HOMO-1})$	−7.61	−7.67
	$E(n_{HOMO-1})$	−7.39	−7.53		$E(n_{HOMO-2})$	−8.88	−8.88
	$E(n)_{av}$	−7.39	−7.53		$E(n)_{av}$	−7.62	−7.66
$\mathbf{4}_{H_2S}$	$E(n_{HOMO})$	−6.67	−6.81		β_{TS}	−0.62	−0.61
	$E(n_{HOMO-1})$	−7.88	−8.05	$\mathbf{10}_{H_2S}$	$E(n_{HOMO})$	−6.69	−6.71
	$E(n)_{av}$	−7.28	−7.43		$E(n_{HOMO-1})$	−6.84	−6.90
	β_{TS}	−0.60	−0.62		$E(n_{HOMO-2})$	−7.64	−7.66
$\mathbf{5}_{H_2S}$	$E(n_{HOMO})$	−6.36	−6.45		$E(n_{HOMO-3})$	−8.36	−8.39
	$E(n_{HOMO-1})$	−7.73	−7.81		$E(n_{HOMO-4})$	−8.50	−8.53
	$E(n)_{av}$	−7.27	−7.36		$E(n)_{av}$	−7.60	−7.64
	β_{TS}	−0.46	−0.45		β_{TS}	−0.42	−0.41
$\mathbf{6}_{H_2S}$	$E(n_{HOMO})$	−6.97	−7.11	$\mathbf{11}_{H_2S}$	$E(n_{HOMO})$	−6.97	−6.96
	$E(n_{HOMO-1})$	−8.60	−8.80		$E(n_{HOMO-1})$	−8.56	−8.54
	$E(n)_{av}$	−7.51	−7.67		$E(n)_{av}$	−7.77	−7.75
	β_{TS}	−0.54	−0.56		β_{TS}	−0.40	−0.39
$\mathbf{7}_{H_2S}$	$E(n_{HOMO})$	−6.62	−6.71				
	$E(n_{HOMO-1})$	−7.50	−7.60				
	$E(n_{HOMO-2})$	−8.32	−8.47				
	$E(n)_{av}$	−7.48	−7.59				
	β_{TS}	−0.60	−0.62				
$\mathbf{8}_{H_2S}$	$E(n_{HOMO})$	−6.62	−6.70				
	$E(n_{HOMO-1})$	−7.08	−7.17				
	$E(n_{HOMO-2})$	−7.98	−8.04				
	$E(n_{HOMO-3})$	−8.49	−8.58				
	$E(n)_{av}$	−7.54	−7.62				
	β_{TS}	−0.46	−0.45				

Splitting in **4** is 0.60 eV, and splitting in the H_2S model system is 1.21 eV, as listed in Tables 2−4. This comparison indicates that 0.48 eV of the TB splitting (1.21−0.73 eV) is caused by interactions due to the central σ_{C-C} bond and only 0.13 eV (0.73−0.60 eV) is due to interaction with the remaining carbon framework.

There are three trithiaadamantane isomers. If the sulfurs are all attached to the same carbon bridgehead, as in **5**, the lone pairs interact identically with the rest of the molecule and with two other sulfurs. This gives the splitting pattern shown in Figure 10, similar to the pattern of the $\mathbf{5}_{H_2S}$ model system. β_{TS} is −0.46 eV. This is opposite to that of a Hückel cyclopropenyl system where there is one stabilized orbital and two that are destabilized. The S lone pairs of **5** constitute a Möbius system with an odd number of negative overlaps. In **5**, the HOMO consists of the antibonding combination of the three lone pairs, and the degenerate HOMO-1s are composed of one net bonding interaction. The all-antibonding HOMO, like the HOMO of **4**, has no $n_S-\sigma_{C-C}$ interaction with the σ_{C-C} bonds behind the sulfurs. In contrast, the doubly degenerate n_S orbitals have significant mixing with σ_{C-C} and σ_{C-S} orbitals that cause them to be pushed up in energy along with the average energy of the lone-pair orbitals. These interactions give a $\Gamma_{H/TB}(n_{HOMO-1})$ of +0.29 eV. Because of additional $n_S \rightarrow \sigma_{C-S}^*$ delocalization interactions, the HOMO of **5** is stabilized more significantly than in **4**; $\Gamma_{H/TB}(n_{HOMO})$ is −0.22 eV.

When the three sulfurs are placed as in **6**, a cyclic array of three lone-pair π-type interactions analogous to a cyclopropenyl system is formed (Figure 11). The orientation of the sulfurs in **6** allows the lobes of each lone pair to interact in a π fashion. This permits an all bonding combination of the lone pairs that, when compared to $\mathbf{6}_{H_2S}$, is stabilized by $2\beta_{TS}$, where β_{TS} is −0.54 eV. The other two orbitals consist mainly of one antibonding combination and are destabilized by β_{TS}. The net splitting pattern of **6** is shown in Figure 11. The doubly degenerate HOMOs have no $n_S-\sigma_{C-C}$ interactions and only minor tilting of the lone-pair orbitals due, in part, to $n_S \rightarrow \sigma_{C-S}^*$ delocalization. The lowest energy lone-pair molecular orbital consists of the bonding combination of all three n_S orbitals with appreciable mixing with adjacent σ_{C-C} orbitals. The destabilizing effects of these TB interactions decrease splitting by raising the energy of the HOMO-1. The differences in geometric orientation of the sulfurs in **5** and **6** significantly alter the strength of the TB interactions. $\Gamma_{H/TB}(n_{HOMO-1})$ for **6** is +1.21 eV, which is approximately four times that of **5**. $\Gamma_{H/TB}(n_{HOMO})$ for **6** is destabilizing by +0.24 eV, while that of **5** was stabilizing by approximately the same amount. This indicates that TB interactions are affected by the relative orientation of the sulfurs, while TS interactions remain fairly constant despite differences in orientation of the sulfurs in **5** and **6**.

Trithiaadamantane **7** consists of two distally located sulfurs interacting with a third sulfur, shown in Figure 12. The Hückel model of $\mathbf{7}_{H_2S}$ comprises three nondegenerate orbitals with two orbitals stabilized or destabilized by $\sqrt{2}\beta_{TS}$, shown in Figure 5. The HOMO-1 is located at α and involves the noninteracting distally located sulfurs, which have been determined in **3** to have net TS interactions of zero. These sulfurs do not interact with each other, though they can mix with proximal σ_{C-C} bonds. The value of β_{TS} is −0.60 eV and is only slightly higher than that of the previous trithiaadamantanes. The HOMO of **7** does not contain significant $n_S-\sigma_{C-C}$ interaction, while the lower energy orbitals contain increasing amounts of $n_S-\sigma_{C-C}$ mixing. Orbital tilting due to $n_S \rightarrow \sigma_{C-S}^*$ hyperconjugation is observed in the HOMO where $\Gamma_{H/TB}(n_{HOMO})$ is −0.26 eV. The HOMO-*n* orbitals are destabilized by $\Gamma_{H/TB}(n_{HOMO-1}) = +0.19$ eV and $\Gamma_{H/TB}(n_{HOMO-2}) = +0.57$ eV due to increased mixing with the carbon framework.

Orbital interactions in tetrathiaadamantane become more complicated due to loss of symmetry. The average energy of the lone pairs continues to lower with the addition of sulfurs. For 2,4,6,10-tetrathiaadamantane (**8**) the average lone-pair orbital energy decreases from −5.68 eV in 2-thiaadamantane to −6.38 eV, and from −7.12 eV in the monomer model system to −7.54 eV for $\mathbf{8}_{H_2S}$. Structure **8** is a cyclic array of three sulfurs as in **7** with a fourth sulfur located distal to one of the sulfurs and proximal to the other two. The corresponding Hückel model of $\mathbf{8}_{H_2S}$ has four nondegenerate orbitals that are stabilized or destabilized by β_{TS} or $2\beta_{TS}$ (Figure 5). In this case, $\beta_{TS} = -0.46$ eV. The correlation diagram for **8** is shown in Figure 13. The HOMO does not interact with the carbon skeleton through bond, and the HOMO-1 exhibits only slight tilting and deformation of the lone pairs involving $n_S \rightarrow \sigma_{C-S}^*$ delocalization. The two stabilized orbitals involve mixing between n_S and σ_{C-C} and σ_{C-S}

TABLE 4: B3LYP Orbital Splitting Energies (eV) of Adamantane and Polythiaadamantanes

		6-31G(d)	6-311+G(d,p)			6-31G(d)	6-311+G(d,p)
2	$E(n_{HOMO})$	−5.68	−5.87	**9**	$E(n_{HOMO})$	−5.74	−5.90
3	$E(n_{HOMO})$	−5.94	−6.13		$E(n_{HOMO-1})$	−6.35	−6.53
	$E(n_{HOMO-1})$	−5.94	−6.13		$E(n_{HOMO-2})$	−7.05	−7.22
	$E(n)_{av}$	−5.94	−6.13		$E(n)_{av}$	−6.38	−6.54
	$E(n_{NBO})$	−6.05	−6.22		$E(n_{NBO})$	−6.47	−6.62
	Δ_{TS+TB}	0.00	0.00		Δ_{TS+TB}	0.61	0.63
	$\Gamma_{H/TB}(n_{HOMO})$	0.11	0.09		Δ_{TS+TB}	0.70	0.69
	$\Gamma_{H/TB}(n_{HOMO-1})$	0.11	0.09		$\Gamma_{H/TB}(n_{HOMO})$	−0.49	−0.53
4	$E(n_{HOMO})$	−5.62	−5.80		$\Gamma_{H/TB}(n_{HOMO-1})$	0.11	0.09
	$E(n_{HOMO-1})$	−6.22	−6.41		$\Gamma_{H/TB}(n_{HOMO-2})$	0.68	0.60
	$E(n)_{av}$	−5.92	−6.11	**10**	$E(n_{HOMO})$	−6.05	−6.19
	$E(n_{NBO})$	−6.21	−6.40		$E(n_{HOMO-1})$	−6.11	−6.26
	Δ_{TS+TB}	0.60	0.61		$E(n_{HOMO-2})$	−6.63	−6.79
	$\Gamma_{H/TB}(n_{HOMO})$	−0.02	−0.02		$E(n_{HOMO-3})$	−7.00	−7.16
	$\Gamma_{H/TB}(n_{HOMO-1})$	0.59	0.61		$E(n_{HOMO-4})$	−7.15	−7.30
5	$E(n_{HOMO})$	−5.56	−5.73		$E(n)_{av}$	−6.59	−6.74
	$E(n_{HOMO-1})$	−6.41	−6.59		$E(n_{NBO})$	−6.76	−6.89
	$E(n)_{av}$	−6.13	−6.30		Δ_{TS+TB}	0.06	0.06
	$E(n_{NBO})$	−6.25	−6.41		Δ_{TS+TB}	0.52	0.53
	Δ_{TS+TB}	0.85	0.86		Δ_{TS+TB}	0.37	0.37
	$\Gamma_{H/TB}(n_{HOMO}$	−0.22	−0.23		Δ_{TS+TB}	0.15	0.14
	$\Gamma_{H/TB}(n_{HOMO-1})$	0.29	0.27		$\Gamma_{H/TB}(n_{HOMO})$	−0.24	−0.26
6	$E(n_{HOMO})$	−5.95	−6.11		$\Gamma_{H/TB}(n_{HOMO-1})$	−0.15	−0.13
	$E(n_{HOMO-1})$	−6.62	−6.81		$\Gamma_{H/TB}(n_{HOMO-2})$	0.12	0.10
	$E(n)_{av}$	−6.17	−6.35		$\Gamma_{H/TB}(n_{HOMO-3})$	0.48	0.45
	$E(n_{NBO})$	−6.74	−6.95		$\Gamma_{H/TB}(n_{HOMO-4})$	0.47	0.46
	Δ_{TS+TB}	0.67	0.70	**11**	$E(n_{HOMO})$	−6.33	−6.46
	$\Gamma_{H/TB}(n_{HOMO}$	0.24	0.27		$E(n_{HOMO-1})$	−7.25	−7.39
	$\Gamma_{H/TB}(n_{HOMO-1})$	1.21	1.26		$E(n)_{av}$	−6.79	−6.93
7	$E(n_{HOMO})$	−5.73	−5.90		$E(n_{NBO})$	−6.88	−6.99
	$E(n_{HOMO-1})$	−6.16	−6.34		Δ_{TS+TB}	0.93	0.93
	$E(n_{HOMO-2})$	−6.60	−6.78		$\Gamma_{H/TB}(n_{HOMO})$	−0.24	−0.26
	$E(n)_{av}$	−6.16	−6.34		$\Gamma_{H/TB}(n_{HOMO-1})$	0.42	0.39
	$E(n_{NBO})$	−6.35	−6.52				
	Δ_{TS+TB}	0.43	0.44				
	Δ_{TS+TB}	0.44	0.44				
	$\Gamma_{H/TB}(n_{HOMO})$	−0.26	−0.27				
	$\Gamma_{H/TB}(n_{HOMO-1})$	0.19	0.18				
	$\Gamma_{H/TB}(n_{HOMO-2})$	0.57	0.60				
8	$E(n_{HOMO})$	−5.84	−5.99				
	$E(n_{HOMO-1})$	−6.15	−6.31				
	$E(n_{HOMO-2})$	−6.68	−6.85				
	$E(n_{HOMO-3})$	−6.84	−7.01				
	$E(n)_{av}$	−6.38	−6.54				
	$E(n_{NBO})$	−6.68	−6.84				
	Δ_{TS+TB}	0.31	0.31				
	Δ_{TS+TB}	0.53	0.54				
	Δ_{TS+TB}	0.15	0.16				
	$\Gamma_{H/TB}(n_{HOMO})$	−0.08	−0.07				
	$\Gamma_{H/TB}(n_{HOMO-1})$	0.07	0.09				
	$\Gamma_{H/TB}(n_{HOMO-2})$	0.43	0.41				
	$\Gamma_{H/TB}(n_{HOMO-3})$	0.79	0.79				

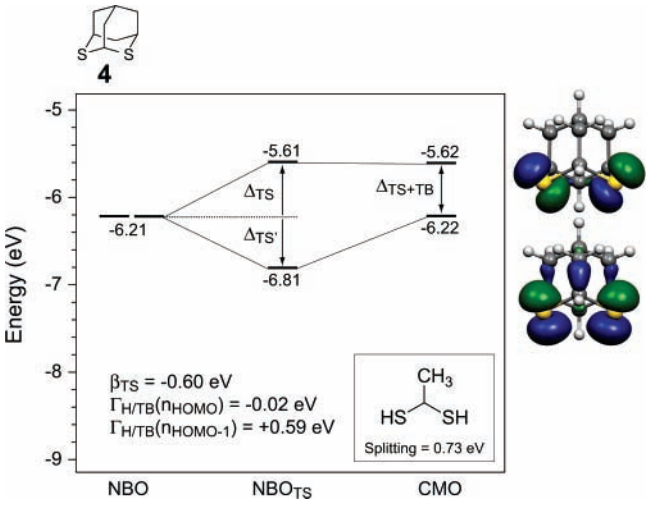

Figure 9. B3LYP/6-31G(d) orbital correlation diagram of 2,4-dithiaadamantane (**4**). The inset shows $CH_3CH(SH)_2$ used for modeling TB interactions with the central σ_{C-C} bond of **4**. Molecular orbital energies are reported in electronvolts.

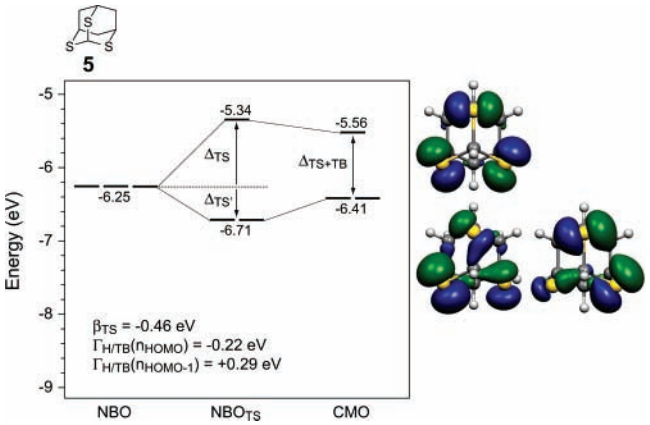

Figure 10. B3LYP/6-31G(d) orbital correlation diagram of 2,4,10-trithiaadamantane (**5**). Molecular orbital energies are reported in electronvolts.

orbitals. The lowest energy orbital contains stronger $n_S-\sigma_{C-C}$ and $n_S-\sigma_{C-S}$ interactions that raise the HOMO-3 energy by +0.79 eV, as indicated by $\Gamma_{H/TB}(n_{HOMO-3})$. The unsymmetrical contribution of TB effects due to increased interaction with the molecular skeleton in the lower energy orbitals is indicated by the unsymmetrical splitting of the orbitals. The HOMO-2 is destabilized by −0.43 eV by TB interactions and ends up being

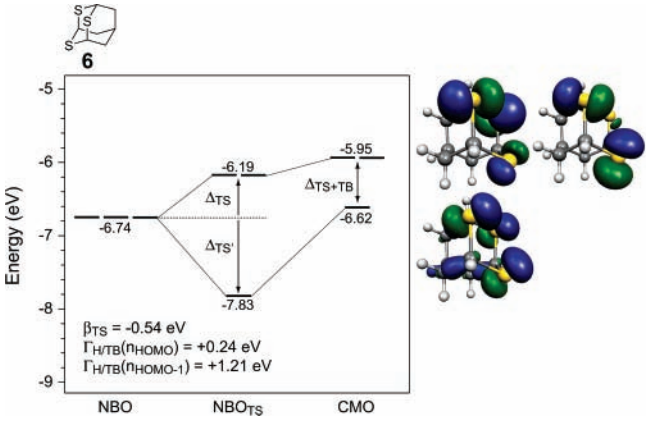

Figure 11. B3LYP/6-31G(d) orbital correlation diagram of 2,4,9-trithiaadamantane (**6**). Molecular orbital energies are reported in electronvolts.

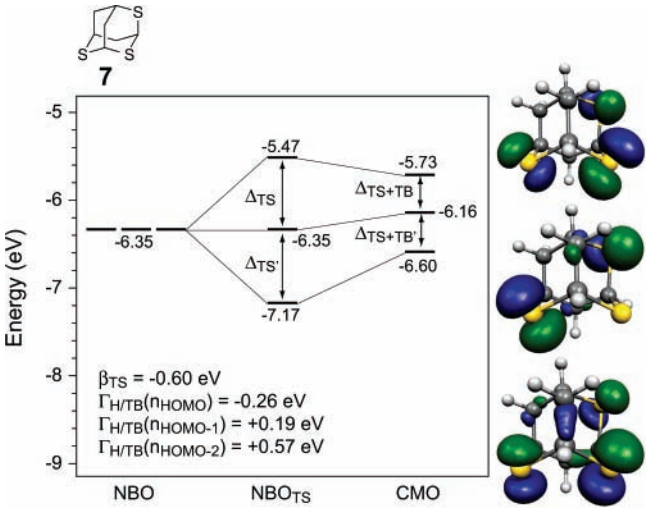

Figure 12. B3LYP/6-31G(d) orbital correlation diagram of 2,4,6-trithiaadamantane (**7**). Molecular orbital energies are reported in electronvolts.

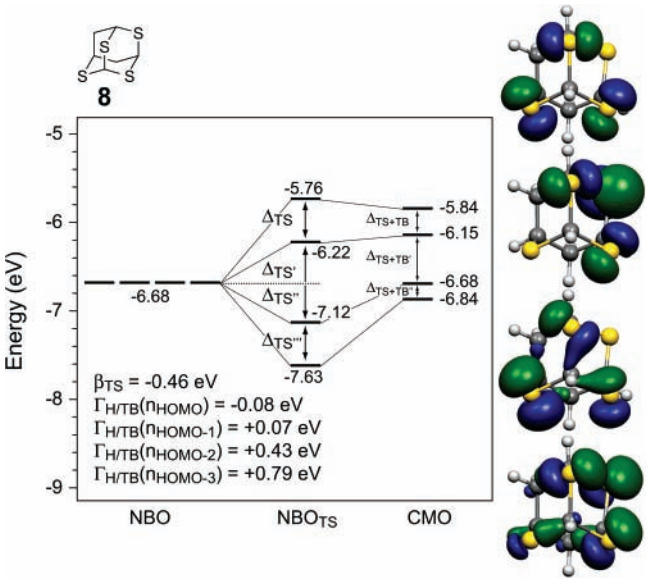

Figure 13. B3LYP/6-31G(d) orbital correlation diagram of 2,4,6,10-tetrathiaadamantane (**8**). Molecular orbital energies are reported in electronvolts.

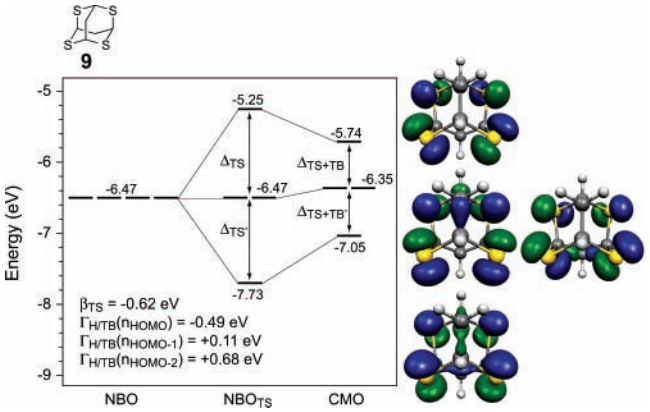

Figure 14. B3LYP/6-31G(d) orbital correlation diagram of 2,4,6,8-tetrathiaadamantane (**9**). Molecular orbital energies are reported in electronvolts.

only 0.16 eV higher than HOMO-3. The splitting energy Δ_{TS+TB} between the HOMO and HOMO-1 is 0.31 eV and is larger because of minimal interactions with the σ skeleton in these orbitals.

The isomer, 2,4,6,8-tetrathiaadamantane (**9**), has a cyclic array of four lone-pair interactions with D_{2d} symmetry. This arrangement results in an orbital splitting pattern identical to that of a Hückel cyclobutadiene system. In this cyclic array, a pure π- or pure σ-type interaction gives the same result. In **9** and $\mathbf{9}_{H_2S}$ the interactions are between pure π- and pure σ-type lone-pair interactions, but both give the familiar Hückel orbital energy pattern. The correlation diagram for $\mathbf{9}_{H_2S}$ is shown in Figure 5. The Hückel model shows that one orbital is stabilized by $2\beta_{TS}$ with all bonding interactions and another is destabilized by $2\beta_{TS}$ with all antibonding interactions. The remaining two orbitals are degenerate and have net zero interaction energy due to the presence of an equal number of bonding and antibonding interactions. The value of β_{TS} determined from this splitting pattern is -0.62 eV. The correlation diagram of **9** is shown in Figure 14. As in **8**, there are no TB interactions in the HOMO of **9**, while TB $n_S-\sigma_{C-C}$ interactions increase from the HOMO-1 to HOMO-2. This is reflected in $\Gamma_{H/TB}$ values of -0.49, $+0.11$, and $+0.68$ eV for the HOMO, HOMO-1, and HOMO-2, respectively.

The 2,4,6,8,9-pentathiaadmantane, **10**, has two types of sulfurs and two types of βs, but the simple Hückel model with all αs and βs equal predicts less splitting than was found experimentally. Hückel analysis of the model system $\mathbf{10}_{H_2S}$ indicate two sets of doubly degenerate orbitals that are stabilized or destabilized by $2\beta_{TS}$ and a single orbital with net interaction energy of zero. The inequivalence of one sulfur leads to a splitting of the degenerate orbitals, shown in $\mathbf{10}_{H_2S}$ in Figure 5. To illustrate that degeneracy is removed and to approximate β_{TS}, the average energies of the near-degenerate orbitals are indicated as dotted lines. This gives $\beta_{TS} = -0.42$ eV, which is the lowest value predicted so far. The geometry of **10** is such that one sulfur interacts with four sulfurs, while each of the other four interact with only three. The lone-pair molecular orbitals and correlation diagram of **10** are shown in Figure 15. The HOMO does not contain significant TB interactions, and $n_S-\sigma_{C-S}$ and $n_S-\sigma_{C-C}$ interactions become more prominent in the HOMO-*n* orbitals. Consistent with the trend established by mono- through tetrathiaadamantane, addition of the fifth sulfur causes the average lone-pair orbital energy of **10** and the H_2S model system to decrease to -6.59 and -7.60 eV, respectively, in comparison to their monosubstituted analogues. When compared to the NBO_{TS} energies, TB effects in **10** cause $\Gamma_{H/TB}$ orbital shifts of -0.24, -0.15, $+0.12$, $+0.48$, and $+0.47$ eV, in order of increasing stability. The near-degenerate HOMO-3 and HOMO-4 have the largest $\Gamma_{H/TB}$ shifts, and the HOMO-2

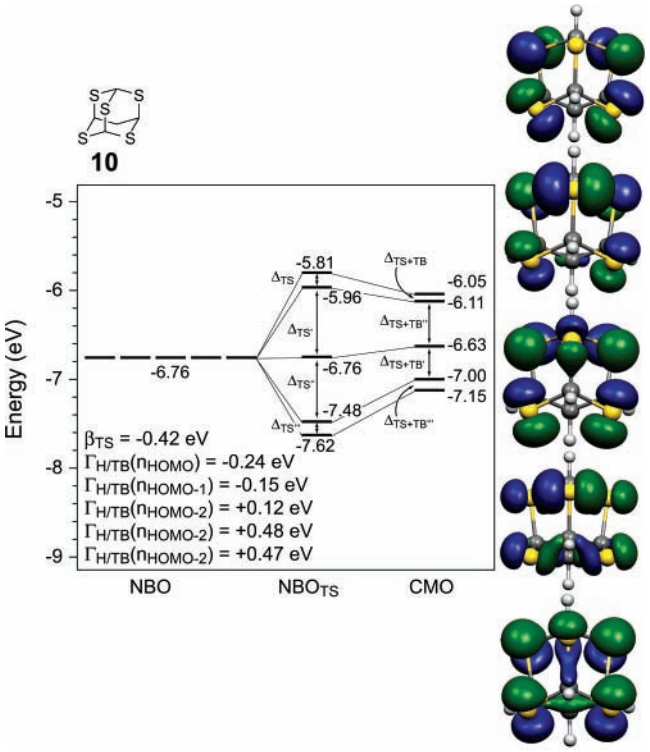

Figure 15. B3LYP/6-31G(d) orbital correlation diagram of 2,4,6,8,9-pentathiaadamantane (**10**). Molecular orbital energies are reported in electronvolts.

is shifted by about half of that value. The HOMO-1 and HOMO are nearly degenerate and stabilized by TB interactions.

Hexasubstituted structure **11** is the final structure in the series of polythiaadamantanes. The 2,4,6,8,9,10-hexathiaadamantane belongs to the same symmetry point group as adamantane, T_d, with the lone-pair orbitals belonging to either the T_1 or T_2 irreducible representations. This provides straightforward results from Hückel analysis of the model system $\mathbf{11}_{H_2S}$; two sets of triply degenerate orbitals are stabilized or destabilized by $2\beta_{TS}$. β_{TS} is calculated to be -0.40 eV. Since all CH_2 groups have been replaced by sulfur atoms in **11**, TS and TB interactions are caused only by mixing with σ_{C-S} orbitals and $n_S \rightarrow \sigma_{C-S}^*$ delocalization. The average energy of the lone pairs of **11** and the model system are inductively lowered to -6.79 and -7.77 eV, respectively. This decrease is the largest in the series of polythiaadamantanes, completing the trend that inductive effects increase as sulfurs are added. The triply degenerate HOMO contains no mixing with the σ-bonds and is stabilized by $\Gamma_{H/TB}(n_{HOMO})$ of -0.24 eV, shown in Figure 16. The HOMO-1 orbitals are destabilized by $+0.42$ eV due to various repulsive interactions with σ_{C-S} bonds.

The orbital energies of polythiaadamantanes are shown to vary depending on the number of sulfurs present and the extent of interaction of the lone pairs with the carbon framework. The average lone-pair orbital energies steadily decrease with an increase in the number of sulfurs, eventually leading to an average orbital energy that is 1.11 eV lower than that of 2-thiaadamantane. Therefore, sulfur acts as the more electronegative element due to increasing TB and TS inductive effects. The orbital splitting due to TS interactions of the sulfurs was approximated using a Hückel model composed of H_2S molecules. From this analysis, the interaction resonance integral due to TS interactions, β_{TS}, varies from -0.60 eV in **4** to -0.40 eV in **11**. The variation of β_{TS} in the series of polythiaadamantanes can be attributed to differences in orientation of the lone-pair orbitals within the caged geometry of the H_2S model systems. For example, the lone-pair orbitals of the H_2S model systems of **10** and **11** extend into the interior of the cage to produce TS interactions different than those in **4** where the lone pairs remain perpendicular to the planes of the H_2S molecules. As a result, β_{TS} varies slightly due to changes in the nature of TS interactions even though S−S distances remain more or less constant in polythiaadamantanes.

Changes in bond lengths and bond angles in going from σ_{C-C} to σ_{C-S} bonds upon replacement of methylene groups have a small effect on the distances between sulfurs. Since TS interactions are expected to fall off rapidly with increasing separation, drastic changes in geometry that alter the S−S interaction distance would cause a noticeable difference in TS splitting. However, when the geometries of different polythiaadamantanes are compared, the S−S distances are not very

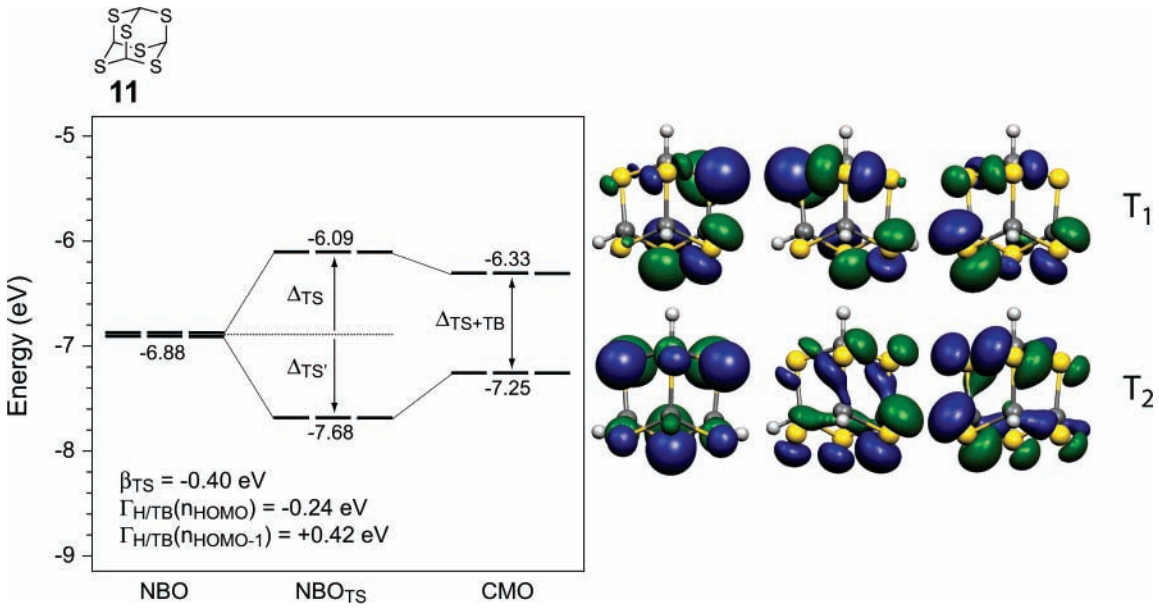

Figure 16. B3LYP/6-31G(d) orbital correlation diagram of 2,4,6,8,9,10-hexathiaadamantane (**11**). Molecular orbital energies are reported in electronvolts. HTA belongs to the T_d symmetry point group with the lone-pair orbitals of sulfur being split into two sets of degenerate orbitals, T_1 and T_2.

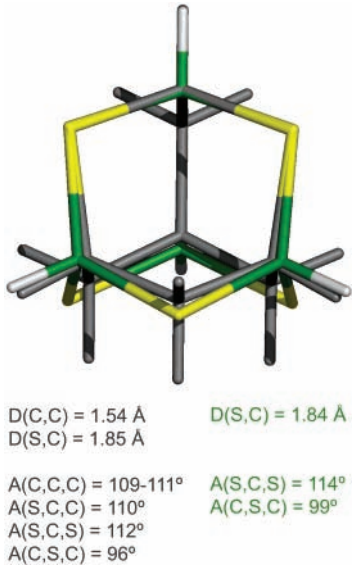

Figure 17. Overlay of 2,4-dithiaadamantane (**4**) and 2,4,6,8,9,10-hexathiaadamantane (**11**) for comparison of geometric parameters. Bond distances are reported in angstroms, and bond angles are reported in degrees.

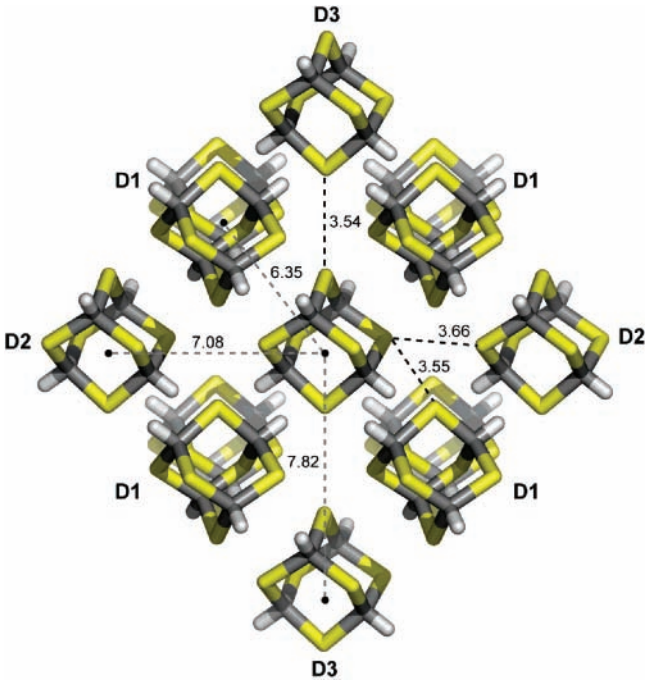

Figure 18. Crystal structure of HTA with center of mass and shortest intermolecular S−S distances reported in angstroms. HTAs that interact with the central HTA by three unique dimer interactions are labeled **D1**, **D2**, and **D3**.

different. The shortest S−S distances in **4**−**11** vary from 3.05 to 3.09 Å. An overlay of **4** and **11** is shown in Figure 17 to demonstrate the relatively small changes in geometry.

Electronic Coupling in HTA Crystals. The crystal structure of HTA has intermolecular S−S distances as short as 3.54 Å, shorter than intramolecular distances between distal sulfurs (4.37 Å) but longer than distances between proximal sulfurs (3.09 Å). A crystal structure of HTA was achieved at good resolution (R value = 1.4%) by the Wudl group[56] and is shown in Figure 18. Intermolecular S−S distances of 3.54 Å and center of mass distances of 6.35 Å are found. The parameters obtained from this crystal structure were used to investigate dimer coupling and to approximate hole mobility. Distally located sulfurs in the crystal structure are on average 4.30 Å apart, and adjacent sulfurs are on average 3.04 Å apart. The corresponding distances obtained from B3LYP/6-31G(d) optimizations are in good agreement at 4.37 and 3.09 Å. To investigate intermolecular electronic coupling in the crystal, dimer interactions were calculated using B3LYP/6-31G(d). The crystal structure shows that each molecule has three unique dimer interactions, labeled **D1**, **D2**, and **D3** in Figure 18, and a total of 14 neighboring molecules with intermolecular S−S distances within 3.7 Å.

TABLE 5: HOMO and HOMO-1 Energies and Electronic Coupling Matrix Elements (V) of 2,4,6,7,9,10-Hexathiaadamantane Dimers Calculated with B3LYP/6-31G(d)

dimer	E_{HOMO} (eV)	E_{HOMO-1} (eV)	V (eV)
D1	−6.171	−6.434	0.132
D2	−6.208	−6.316	0.054
D3	−6.307	−6.307	0.000

It is possible to approximate charge transport properties for organic molecules using structures and energies available from DFT calculations. An incoherent hopping model where charge transfer only occurs between neighbors has been used previously for organic semiconductors.[57,58] If each hopping event is considered to be a nonadiabatic transfer reaction, standard Marcus theory can be used to express the hopping rate between neighboring molecules as a function of reorganization energy (λ) and the coupling matrix element (V),[59,60] both of which can be obtained computationally.[61] This model for calculating hole mobilities is meant to be a computational estimate, while the important quantities are the electronic coupling matrix elements that are an indication of hole mobility and the strength of coupling between molecular units. The orbital energies calculated for the dimer can be used to approximate the electron-transfer coupling matrix element (V) within the Marcus−Hush two-state model.[59,60,62,63] The coupling matrix element, V, is determined from the splitting energy between the HOMO and HOMO-1 of the dimer. The reorganization energy, λ, is taken as the energy due only to relaxation of the molecular geometry associated with charge transfer and does not include reorganization of the rest of the crystal. Under this assumption, λ for HTA is 0.22 eV. The coupling matrix elements for each dimer interaction were calculated and result in a predicted maximum hole mobility of 1.82 $cm^2/(V\cdot s)$. Coupling energies for the **D1** and **D2** dimers were 0.13 and 0.05 eV, respectively, and are listed in Table 5. No coupling was found to occur in the **D3** dimer since the lone pairs have different symmetries, just as the distally located sulfurs in 2,6-dithiaadamantane do not interact. The S−S distance in **D3** is 3.54 Å, but the lone-pair orbitals are orthogonal. A hole mobility significantly less than 1.82 $cm^2/(V\cdot s)$ would most likely be observed experimentally due to crystal imperfections and other factors such as charge injection, type of substrate, and deposition method. Pentacene has been found to have large carrier mobilities due to the electronic structure of its single crystal[64−66] and remarkably low vibrational reorganization energy.[67] For comparison, hole mobilities as high as 5 $cm^2/(V\cdot s)$ have been predicted for organic semiconductors such as pentacene.[58]

Conclusions

DFT calculations in conjunction with Hückel analysis and NBO analysis of the interactions between sulfur lone-pair orbitals have been used to explain the electronic properties and orbital splitting patterns of polythiaadamantanes. In an attempt to incorporate single HTA crystals into semiconducting devices, it was discovered that polythiaadamantanes were difficult to oxidize despite having an apparent electron-rich system of lone

pair electrons. Consistent with experimental evidence, the IP of HTA was calculated to be 8.36 eV, which is approximately 1 eV lower than the calculated value for adamantane. The IPs of polythiaadamantanes were calculated to be as low as 7.74 eV. An overall decrease in the average energy of the lone pairs is predicted, with the exact positioning of the HOMO depending on specific lone-pair interactions. Cumulative inductive effects of sulfur atoms on each other are responsible for the surprisingly high ionization potential of HTA. In general, B3LYP/6-31G(d) and B3LYP/6-311+G(d,p) give very similar orbital energies and splittings. NBO analysis in conjunction with a model system based on interacting hydrogen sulfide molecules was used to separate TB and TS interactions; TB interations were found to reduce orbital splitting, while TS interactions increase orbital splitting. The TS interaction energy between proximal sulfur atoms in polythiaadamantanes was determined from the resonance integral, β_{TS}, extracted from Hückel analysis of B3LYP/6-31G(d) orbital energies of H_2S model systems. TS interactions were found to be fairly constant from one polythiaadamantane to the next, and the contributions of TB effects to individual orbital energies vary depending on the relative orientation of sulfur atoms. Investigation of dimer pair interactions reveal that electronic coupling is not as strong as expected given the short intermolecular S−S distances observed in the crystal structure. A hole mobility for HTA lower than that predicted for other organic semiconducting crystals such as pentacene was calculated.

Acknowledgment. We are grateful to the National Science Foundation (NSF) for financial support (Grant CHE-0240203). This research was facilitated through the Partnerships for Advanced Computational Infrastructure (PACI) through the support of the NSF. Computations were performed on the NSF Terascale Computing System at the Pittsburgh Supercomputing Center (PSC) and on the UCLA Academic Technology Services (ATS) Hoffman Beowulf cluster. J.E.N. also acknowledges the Integrative Graduate Education and Research Traineeship program supported by the NSF at UCLA for financial support.

Supporting Information Available: Details of computational procedure, Cartesian coordinates, electronic energies, details of Hückel model analysis and prediction of hole mobilities, and the complete ref 32. This material is available free of charge via the Internet at http://pubs.acs.org.

References and Notes

(1) Hoffmann, R. *Acc. Chem. Res.* **1971**, *4*, 1−9.
(2) Hoffmann, R.; Heilbronner, E.; Gleiter, R. *J. Am. Chem. Soc.* **1970**, *92*, 706−707.
(3) Hoffmann, R.; Imamura, A.; Hehre, W. J. *J. Am. Chem. Soc.* **1968**, *90*, 1499−1509.
(4) Squires, R. R.; Cramer, C. J. *J. Phys. Chem. A* **1998**, *102*, 9072−9081.
(5) Winkler, M. *J. Phys. Chem. A* **2005**, *109*, 1240−1246.
(6) Paddon-Row: M. N.; Shephard, M. J. *J. Am. Chem. Soc.* **1997**, *119*, 5355−5365.
(7) Falcetta, M. F.; Jordan, K. D.; McMurry, J. E.; Paddon-Row: M. N. *J. Am. Chem. Soc.* **1990**, *112*, 579−586.
(8) Dewar, M. J. S.; Wasson, J. S. *J. Am. Chem. Soc.* **1970**, *92*, 3506−3508.
(9) Heilbronner, E. *Isr. J. Chem.* **1972**, *10*, 143−156.
(10) Heilbronner, E.; Schmelzer, A. *Helv. Chim. Acta* **1975**, *58*, 936−967.
(11) Jordan, K. D.; Michejda, J. A.; Burrow, P. D. *Chem. Phys. Lett.* **1976**, *42*, 227−231.
(12) Bischof, P.; Hashmall, J. A.; Heilbronner, E.; Hornung, V. *Helv. Chim. Acta* **1969**, *52*, 1745−1749.
(13) Heilbronner, E.; Martin, H. D. *Helv. Chim. Acta* **1972**, *55*, 1490−1502.
(14) Paddon-Row: M. N.; Wong, S. S.; Jordan, K. D. *J. Am. Chem. Soc.* **1990**, *112*, 1710−1722.
(15) Reed, A. E.; Curtiss, L. A.; Weinhold, F. *Chem. Rev.* **1988**, *88*, 899−926.
(16) Reed, A. E.; Weinstock, R. B.; Weinhold, F. *J. Chem. Phys.* **1985**, *83*, 735−746.
(17) Reed, A. E.; Weinhold, F. *J. Chem. Phys.* **1985**, *83*, 1736−1740.
(18) Reed, A. E.; Weinhold, F. *J. Chem. Phys.* **1983**, *78*, 4066−4073.
(19) Chong, D. P.; Gritsenko, O. V.; Baerends, E. J. *J. Chem. Phys.* **2002**, *116*, 1760−1772.
(20) Stowasser, R.; Hoffmann, R. *J. Am. Chem. Soc.* **1999**, *121*, 3414−3420.
(21) Politzer, P.; Abu-Awwad, F. *Theor. Chem. Acc.* **1998**, *99*, 83−87.
(22) Baerends, E. J.; Gritsenko, O. V. *J. Phys. Chem. A* **1997**, *101*, 5383−5403.
(23) Baerends, E. J. *Theor. Chem. Acc.* **2000**, *103*, 265−269.
(24) Baerends, E. J.; Gritsenko, O. V.; van Leeuwen, R. *Chemical Applications of Density Functional Theory*; American Chemical Society: Washington, DC, 1996.
(25) Bickelhaupt, F. M.; Baerends, E. J. *Rev. Comput. Chem.* **2000**, *15*, 1−86.
(26) Fredga, A.; Olsson, K. *Ark. Kemi* **1956**, *9*, 163−168.
(27) Andersen, E. K.; Lindqvist, I. *Ark. Kemi* **1956**, *9*, 169−173.
(28) The crystal structure of adamantane was obtained from the Cambridge Structural Database.
(29) Shaffer, P. A., Jr. *J. Am. Chem. Soc.* **1947**, *69*, 1557−1561.
(30) Nowacki, W. *Helv. Chim. Acta* **1945**, *28*, 1233−1242.
(31) Ludy-Tenger, F. *Pharm. Acta Helv.* **1949**, *24*, 16−19.
(32) Frisch, M. J.; et al. *Gaussian 03*; Gaussian, Inc.: Wallingford, CT, 2004.
(33) Becke, A. D. *J. Chem. Phys.* **1993**, *98*, 5648−5652.
(34) Lee, C.; Yang, W.; Parr, R. G. *Phys. Rev. B: Condens. Matter Mater. Phys.* **1988**, *37*, 785−789.
(35) Koopmans, T. *Physica (The Hague)* **1933**, *1*, 104−13.
(36) Unpublished electrochemical data and characterization of HTA-based field-effect transistor (FET) devices have been performed by A.L.B. of the Wudl group.
(37) Kim, K.; Jordan, K. D.; Paddon-Row: M. N. *J. Phys. Chem.* **1994**, *98*, 11053−11058.
(38) Lemierre, V.; Chrostowska, A.; Dargelos, A.; Chermette, H. *J. Phys. Chem. A* **2005**, *109*, 8348−8355.
(39) Gleiter, R.; Spanget-Larsen, J. *Top. Curr. Chem.* **1979**, *86*, 139−195.
(40) Bock, H.; Wagner, G. *Angew. Chem., Int. Ed. Engl.* **1972**, *11*, 150−151.
(41) Wagner, G.; Bock, H. *Chem. Ber.* **1974**, *107*, 68−77.
(42) Frost, D. C.; Herring, F. G.; Katrib, A.; McDowell, C. A.; McLean, R. A. N. *J. Phys. Chem.* **1972**, *76*, 1030−1034.
(43) Khvostenko, V. I.; Furlei, I. I. *Zh. Fiz. Khim.* **1968**, *42*, 13−16.
(44) Bock, H.; Wagner, G.; Kroner, J. *Tetrahedron Lett.* **1971**, 3713−3719.
(45) Akopyan, M. E. *Zh. Fiz. Khim.* **1970**, *44*, 2918−2919.
(46) Hückel, E. *Z. Phys.* **1931**, *70*, 203−286.
(47) Hückel, E. *Z. Elektrochem. Angew. Phys. Chem.* **1937**, *43*, 752−788.
(48) Hückel, E. *Grundzüge der Theorie Ungesättigter und Aromatischer Verbindungen*; Verlag Chemie, G.m.b.H.: Berlin, 1938.
(49) For a description of the Hückel model and the predicted splitting patterns and energies of the sulfur lone-pair orbitals, see the Supporting Information.
(50) Shephard, M. J.; Paddon-Row: M. N.; Jordan, K. D. *J. Am. Chem. Soc.* **1994**, *116*, 5328−5333.
(51) Jordan, K. D.; Paddon-Row: M. N. *Chem. Rev.* **1992**, *92*, 395−410.
(52) Naleway, C. A.; Curtiss, L. A.; Miller, J. R. *J. Phys. Chem.* **1991**, *95*, 8434−8437.
(53) Curtiss, L. A.; Naleway, C. A.; Miller, J. R. *J. Phys. Chem.* **1993**, *97*, 4059−4063.
(54) Liang, C.; Newton, M. D. *J. Phys. Chem.* **1992**, *96*, 2855−2866.
(55) McKinley, A. J.; Ibrahim, P. N.; Balaji, V.; Michl, J. *J. Am. Chem. Soc.* **1992**, *114*, 10631−10637.
(56) A crystal structure of hexathiaadamantane achieved at a resolution with R value = 1.4% was provided by the Wudl group and is reported in the Supporting Information.
(57) Berlin, Y. A.; Hutchison, G. R.; Rempala, P.; Ratner, M. A.; Michl, J. *J. Phys. Chem. A* **2003**, *107*, 3970−3980.
(58) Deng, W.-Q.; Goddard, W. A., III. *J. Phys. Chem. B* **2004**, *108*, 8614−8621.
(59) Marcus, R. A. *J. Chem. Phys.* **1956**, *24*, 966−978.
(60) Marcus, R. A.; Eyring, H. *Annu. Rev. Phys. Chem.* **1964**, *15*, 155−196.
(61) For a detailed description of the equations and procedures used for predicting hole mobilities, see the Supporting Information.
(62) Hush, N. S. *J. Chem. Phys.* **1958**, *28*, 962−972.
(63) Hush, N. S. *Trans. Faraday Soc.* **1961**, *57*, 557−980.

(64) Cornil, J.; Calbert, J. P.; Brédas, J. L. *J. Am. Chem. Soc.* **2001**, *123*, 1250−1251.
(65) Coropceanu, V.; Malagoli, M.; da Silva Filho, D. A.; Gruhn, N. E.; Bill, T. G.; Brédas, J. L. *Phys. Rev. Lett.* **2002**, *89*, 275503/1−275503/4.
(66) Cheng, Y. C.; Silbey, R. J.; da Silva Filho, D. A.; Calbert, J. P.; Cornil, J.; Brédas, J. L. *J. Chem. Phys.* **2003**, *118*, 3764−3774.
(67) Gruhn, N. E.; da Silva Filho, D. A.; Bill, T. G.; Malagoli, M.; Coropceanu, V.; Kahn, A.; Brédas, J. L. *J. Am. Chem. Soc.* **2002**, *124*, 7918−7919.